



Hydro-chemical and geophysical studies of salinization of the Pliocene–Quaternary aquifer in the zone of El Berka, Moulares-Redayef mining region, Southwest Tunisia

Marwa Ghaib^{1,2} · AbdelKader Mhamdi^{1,2} · Mouez Gouasmia^{1,2} · Damien Delvaux³ · Lahmadi Mourni⁴ · Mohamed Soussi²

Received: 25 May 2022 / Accepted: 11 February 2023 / Published online: 22 March 2023
© Saudi Society for Geosciences and Springer Nature Switzerland AG 2023

Abstract

Groundwater salinization and pollution are widespread phenomena that degrade water quality and endanger future water exploitation. The problem is intensified in aquifers where human activities result in accelerating water quality deterioration, particularly in arid regions. The elevated salinity can also originate from other natural or anthropogenic processes. In the El Berka region Moulares-Redayef mining basin, water quantity and quality are significant concerns. This study was undertaken to identify, detect, and delineate the sources and extent of salinization of the Pliocene–Quaternary groundwater in El Berka region, using a multi-disciplinary study integrating hydro-geochemical approaches. The aquifer is mainly characterized by high salinity waters (2 to 13 g/L) compared to the surrounding aquifers. The salinity of the groundwater is also impacted by the dissolution of evaporate minerals (anhydrite, gypsum, and halite) in the aquifer. The geophysical approach made it possible to determine the extent of salinity in two particular areas. The first one, located near the mountainous areas and the Tabeditt wadi (valley), is characterized by relatively high resistance, which confirms its low salinity. The second area, in the center of the plain, is dominated by very low resistivity showing the presence of saline water. This study is intended to guide for decision-makers and planners in the water sector in managing groundwater quality.

Keywords El Berka · Electrical resistivity tomography · Hydrochemistry · Pliocene–Quaternary aquifer · Salinization

Responsible Editor: Broder J. Merkel

✉ AbdelKader Mhamdi
mha_kada@yahoo.fr

Marwa Ghaib
marwaghaib093@gmail.com

- ¹ Département Des Sciences de La Terre, Faculté Des Sciences de Gafsa, Université de Gafsa, Campus Universitaire Sidi Ahmed Zarrouk, 2112 Gafsa, Tunisia
- ² LR18ES07, Laboratoire Bassins Sédimentaires Et Géologie du Pétrole, Faculté Des Sciences de Tunis, Université de Tunis El Manar, Tunis, Tunisia
- ³ Service Géodynamique Et Ressources Minérales du Département Des Sciences de La Terre Au Musée Royal de L'Afrique Centrale, Tervuren, Belgium
- ⁴ Arrondissement Des Ressources en Eau de Gafsa, Gafsa, Tunisia

Introduction

Groundwater is considered one of the most critical water resources in Tunisia. Due to rain shortage and high population in the last years, well excavation and groundwater use for different purposes have increased without planning. This is a great challenge for this region.

Moreover, this scarcity of water resources in this region is unfortunately combined with severe deterioration of groundwater quality due to salinity. The main objective of this study was to identify the main sources of groundwater salinity and the major hydro-geochemical processes controlling groundwater chemistry in the El Berka region. For example, the presence of evaporates in some cases causes salinization of the water table (Masce et al. 1986). In coastal aquifers, marine intrusion may occur due to over-exploitation of the aquifers (Mamou 1990; Shtivelman et Goldman 2000; Fedrigoni et al. 2001; Panteleit et al. 2001; Pulido et al. 2003; Trabelsi et al. 2005). Other aquifers could be contaminated by salinization from the bedrock (Zouari et al. 2003; Krimissa et al. 2004). The encroachment

of brines from sabkhas (Brayant et al. 1994) and shallow water could result in the mineralization of groundwater (Zammouri et al. 2007; Tarki et al. 2011; 2012). Ascending salt water from a deep aquifer across faults is also possible (Zouari et al. 2003; Kraiem et al. 2015). Under some conditions, evaporation may increase groundwater salinity (Mokadem et al. 2015; Tizro and Voudouris 2008; Moussaoui et al. 2018).

This paper integrates geochemical behavior and geophysical data (electrical tomography, used for the first time in the area) to determine the source and the spatial extent of salinization in the Pliocene–Quaternary aquifer in the El Berka region. This paper also develops a conceptual model of the salinization phenomenon.

Geology and hydrology setting

The investigated area is located in the Southern Atlas Mountains in Southwest Tunisia, approximately 40 km northwest the town of Gafsa (Fig. 1). An arid climate characterizes

this region, with evaporation that exceeds precipitation on average (CRDA Gafsa, 2018). It is the site of increasing agricultural activities, which results in an increased demand for water resources and a gradual deterioration in the chemical quality of these waters (Karaoui et al. 2008; Gouasmia 2008; Hamed et al. 2014). Pliocene–Quaternary sands from the primary surficial aquifer have become progressively more saline during recent decades. The study area is located in Moulares-Redayef mining basin (Fig. 2), where phosphate is mined from the Paleocene–Eocene strata (Sassi 1974). It covers about 300 km² (Omrane et al. 2016) and is bounded to the north by the city of Moulares, to the east by Douara region, to the south by mountain Alima, and to the west by the region of Tabeddit (Fig. 2).

It is part of the Atlas fold and thrust belt, characterized by E–W trending anticlines and synclines and NW–trending strike-slip faults (Soumaya et al. 2020). The strike-slip faults of Gafsa, Negrine, and Metlaoui are active and prone to strong earthquakes (Soumaya et al. 2015). From the distribution of the epicenters and focal mechanism solutions,

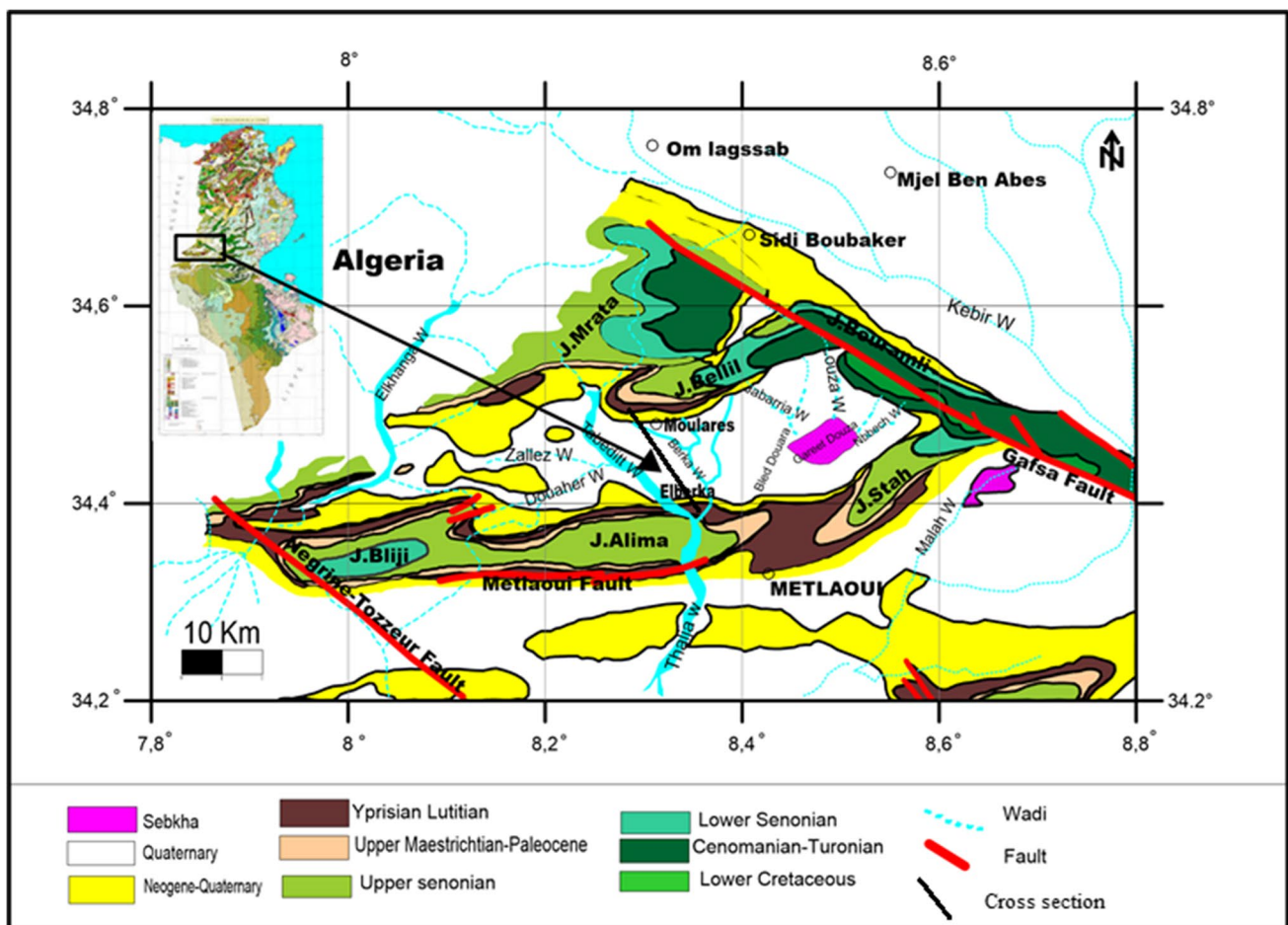
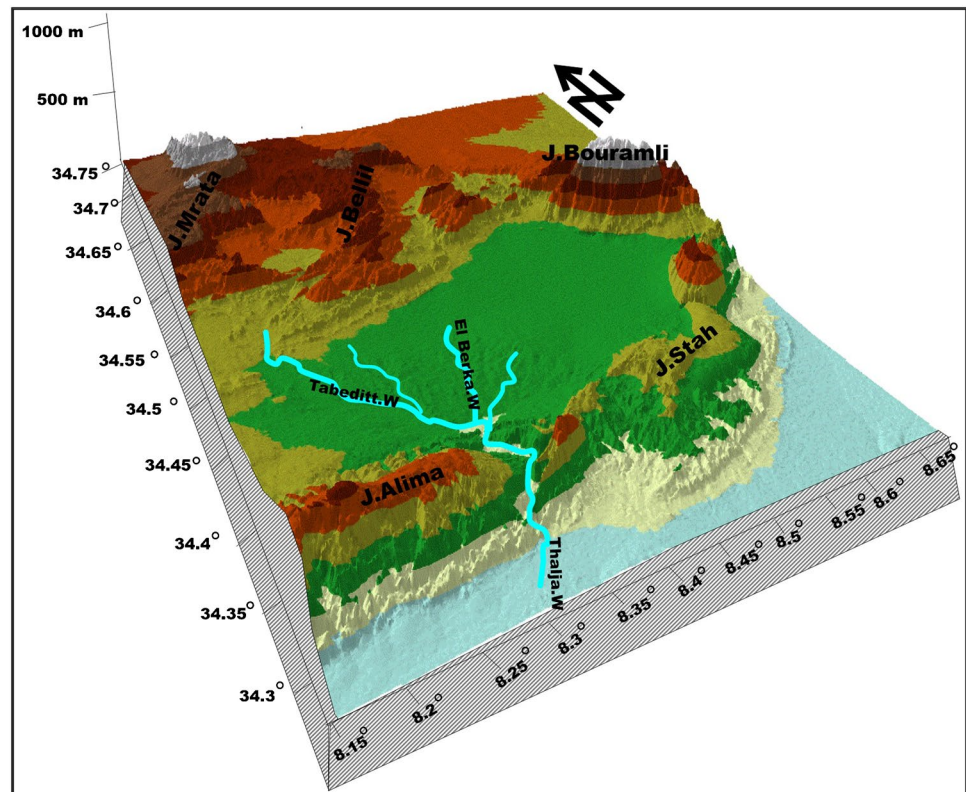


Fig. 1 Geological map and location of the study area (extract from the geological map of Tunisia to 1/500.000 publication of the national geological service)

Fig. 2 A shaded-relief topographic map with the morphology of the study area



the dominant activity is centered on the NW-trending Gafsa and Metlaoui faults (Soumaya et al. 2018).

The structure of the entire Southern Atlas is linked to the interplay of two major deformation corridors (Zargouni 1984):

The corridor of the recess of Gafsa's fault is in the north, which extends from the chain of Tebessa in Algeria to the coastal plain of Gabes (Fig. 1).

The corridor in the south of Chebika, whose existence is linked to the Tozeur-Negrine accident (Fig. 1).

During the Cenozoic era, this area was affected by strike-slip tectonic reactivation, resulting in pull-apart basins bordered by E-W and NW–SE trans-tensional faults (Fig. 3) (Soumaya et al. 2020).

The stratigraphy of the study area is relatively well-known (Swezey 1996, 2003; Riley et al. 2011; Ahmadi et al. 2013; Ben Hassen et al. 2014; Gharbi et al. 2015; Masrouhi et al. 2019; Haji et al. 2020). The stratigraphic units exposed in the study area extend from the Upper Cretaceous to the Quaternary (Fig. 5). The oldest ones belong to the Cenomanian–lower Turonian Zebbag formation. They are composed of clay units at the base, intercalated with numerous carbonate and anhydrite horizons ranging from 580 to 650 m thick. Layers of gypsum marl and clay-limestone characterize the Lower Campanian Upper Turonian Aleg formation (450–500 m thick). The Campanian–Maastrichtian Berda

formation (250–300 m) consists of three parts: the Lower Berda limestone and marl-limestone, the Middle Berda marls and limestone, and the Upper Berda white limestone and blackish green clays. The Paleocene El Haria formation (40–60 m thick) consists of limestone and clay stone. The Metlaoui group, which consists of three formations, represents the Upper Paleocene to Lower Eocene: the Upper Paleocene Selja formation (60–80 m thick) with dolomite and gypsum fossiliferous clay, the Lower Ypresian Chouabine formation (10–30 m thick) with phosphate and phosphate limestone, and the Upper Ypresian Kef Eddour formation (35–40 m thick) composed of fossiliferous limestone (Ahmadi et al. 2013).

Lutetian age series is composed of white dolomite at the base and massive gypsum of the Jebbs formation (gypsum 20–60 m thick). The Oligocene Sehib formation (10–60 m thick) is composed of silt and clay sandstone with locally thick conglomerates at the base. The Miocene is represented by the Beglia formation (10–190 m), which consists of sands of various particle sizes with clay beds at the top. The following Segui formation is represented by a basal conglomerate surmounted by thick series of red clay, gypsum, and intercalation of sandy clay levels (10 to 20 m thick) (Ahmadi et al. 2013). The Quaternary forms thick accumulations of gravel and coarse sands in front of the mountain ranges and gradually thins towards the center of the basin, evolving towards finer sands and clays.

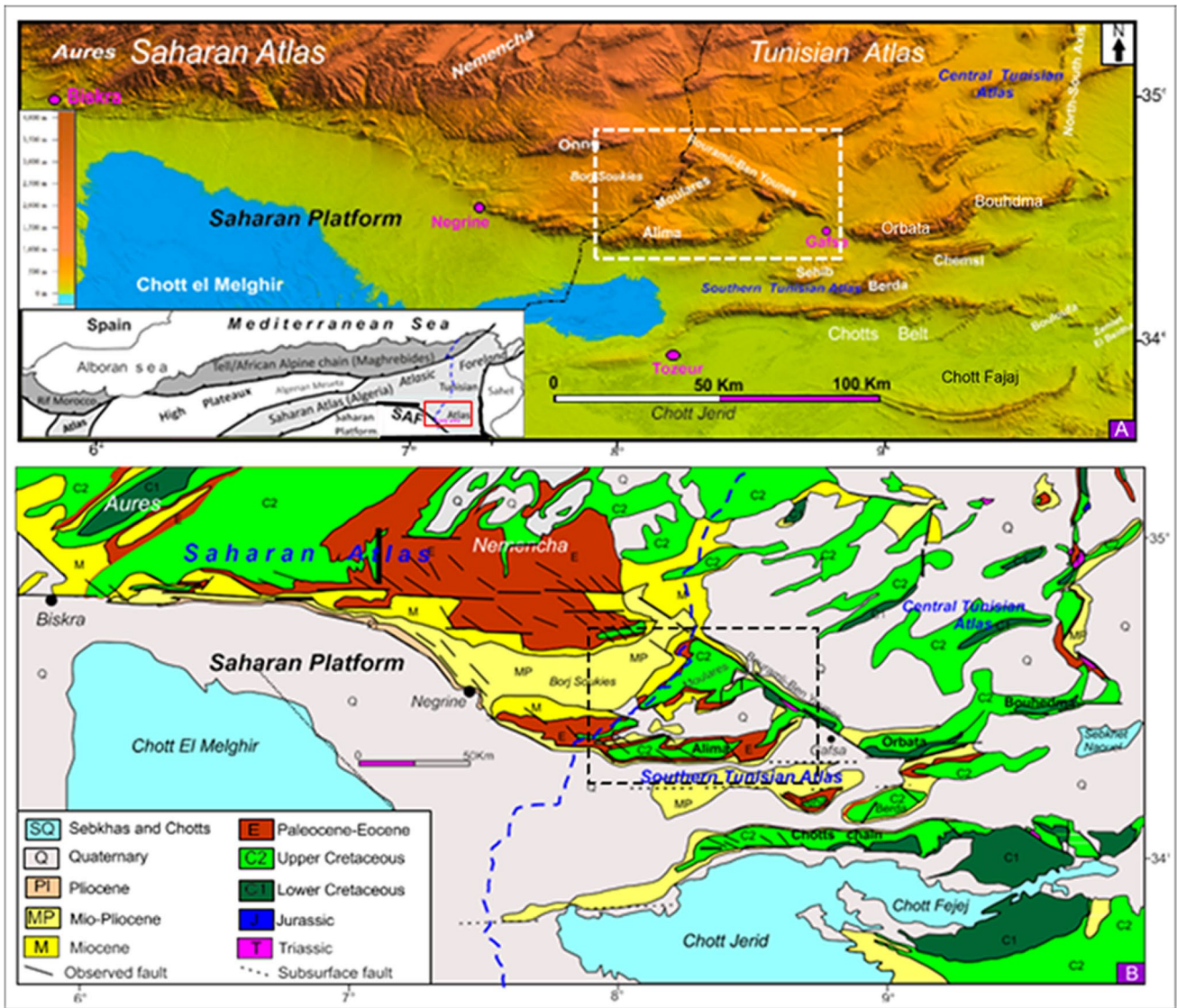


Fig. 3 Structural framework of North Africa Alpine belt and its interpolate Atlas foreland (Soumaya et al. 2020)

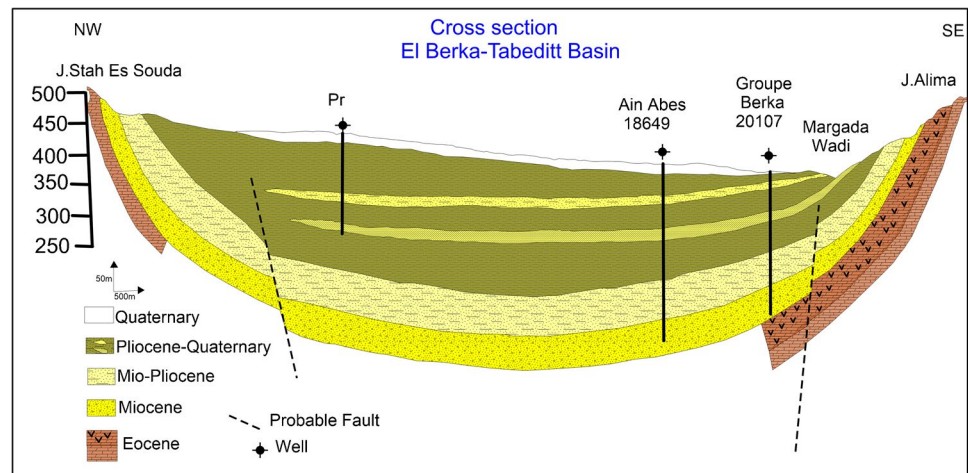
The aquifer of the Moulares-Redayef basin is composed of two main water tables whose piezometric levels have been determined (Farhat 1984; Gouasmia 2008; Karaouli et al. 2008; Hamed et al. 2014):

The Miocene sand aquifer (Figs. 4 and 5) (Begli formation) in the western basin is with an average thickness of about 200 m and reaches 400 m at the center of the basin (Tabeddit region).

The clay-sandy aquifer of Pliocene–Quaternary (Segui formation) (Figs. 4 and 5) in the eastern basin, with an average thickness of about 170 m and reaching 250 m thick at the level of Garâat Douza.

There is also a phreatic and a deep aquifer, but the primary aquifer is a shallow aquifer of Pliocene–Quaternary sands (Gouasmia 2008). Sandy-clay alluvial formations limit the groundwater. These levels captured by the surface wells form the same geological entity as the deep aquifer’s reservoir level, which is separated by impermeable intrusions. However, there is an alluvial layer in the coarse alluvial deposits of the wadi (valley), fed by surface water infiltration (Gouasmia 2008). The natural recharge of the Pliocene–Quaternary groundwater table in the study area is achieved by direct infiltration of rainwater and wadi (valley) flooding. We can conclude from our study that it allows us to identify and estimate the lithology and thickness of surface aquifer formations, delineating the saturated zone and define zones according to their estimated salinity from the measured resistivity (Fig. 6).

Fig. 4 Cross section El Berka Tabeditt Basin



Materials and methods

Sampling and hydrochemical analysis

A total of 26 water samples were collected from the central hydrogeological units of the survey area (water wells in Pliocene–Quaternary sediments (Fig. 7)). All samples were collected from currently exploited wells in order to ensure that water is representative of actual aquifer conditions.

Temperature (T°), pH, and electrical conductivity (EC) were measured in situ using multi-parameter equipment (Table 1). Water analyses were carried out in the laboratory of the Company of Phosphate of Gafsa (CPG) in Tunisia for the following major elements: Ca^{2+} , Mg^{2+} , Na^{+} , K^{+} , Cl^{-} , SO_4^{2-} , HCO_3^{-} , and NO_3^{-} (Table 1). The volumetric technique is used for the measuring Ca^{2+} , Mg^{2+} , Cl^{-} , and HCO_3^{-} , and the atomic absorption spectrophotometry was used for Na^{+} , K^{+} , SO_4^{2-} , and NO_3^{-} .

Golden Software Surfer 10 is used as a mapping tool to display the spatial distribution of chemical elements. The standard methods of Schoeller-Berkaloff (Schoeller 1965) and the Piper classification (Piper 1994) were used to determine the main chemical facies and relations of waters. The principal elements were compared using Excel 7 to delineate the main groundwater salinization processes. Thus, the multivariate statistical approach helps in the interpretation of hydrochemical XLSTAT variables using software for the analysis of the main components (APC) and the hierarchical group (HCA) (Davis 1986). The measurements of statistical levels of water wells are used to draw a piezometric map of the study area (Fig. 8).

Electrical resistivity tomography (ERT)

Generally, geophysical methods are satisfactory for exploring groundwater resources (Oyedele 2009). In particular, geoelectric methods have been widely used to assess groundwater

quality hosted in different lithologies and under different conditions. Compared to other geophysical methods, geoelectric methods are characterized by light equipment, easy implementation, and faster and more economical data analysis (Ekine and Osobonye 1996; Ebraheem et al. 1997; Sikandar et al. 2010). Electrical conductivity and resistivity are intrinsic properties of groundwater chemistry in that they can provide information on the degree of contamination (Delleur et al. 2006; Sherif et al. 2006). Therefore, these methods can be used to delineate the distribution of fresh and saltwater in aquifer systems while identifying the potential for contamination (e.g., Song et al. 2007; Sikandar et al. 2010 a; 2010b; Chongo et al. 2011; Nejad et al. 2011; Mhamdi et al. 2015).

The geo-electrical data, together with the hydrochemical analyses, play a crucially important role in (1) identifying the impact of over-exploitation on the PQ water table, (2) characterizing and interpreting the spatial and vertical variability of the PQ aquifer resistivity features, (3) recognizing the hydrochemical groundwater facies, and (4) identifying the main groundwater mineralization processes. In light of the work undertaken in the study area, the investigation guides how regional decision-makers can prioritize policies and interventions to overcome water constraints in agriculture while ensuring efficient and sustainable water resource management and equitable access to water (Mhamdi et al. 2022).

Electrical imaging is the multidimensional representation or distribution of the intrinsic electrical properties of the medium studied using quadrupoles (Marescot 2004; Griffiths et al. 1993). An electric current is injected into two electrodes, A and B. This current generates an electric field that depends on the conductivity distribution of the underlying terrains. Two electrodes, M and N, record the value of the potential difference (ddp) created by the electric field. It is then possible to reduce the apparent resistivity value of the basement, knowing the geometry of the electrodes, the intensity of the injected current, and the ddp. The apparent resistivity, ρ_a , represents the ratio between the potential measured in the field,

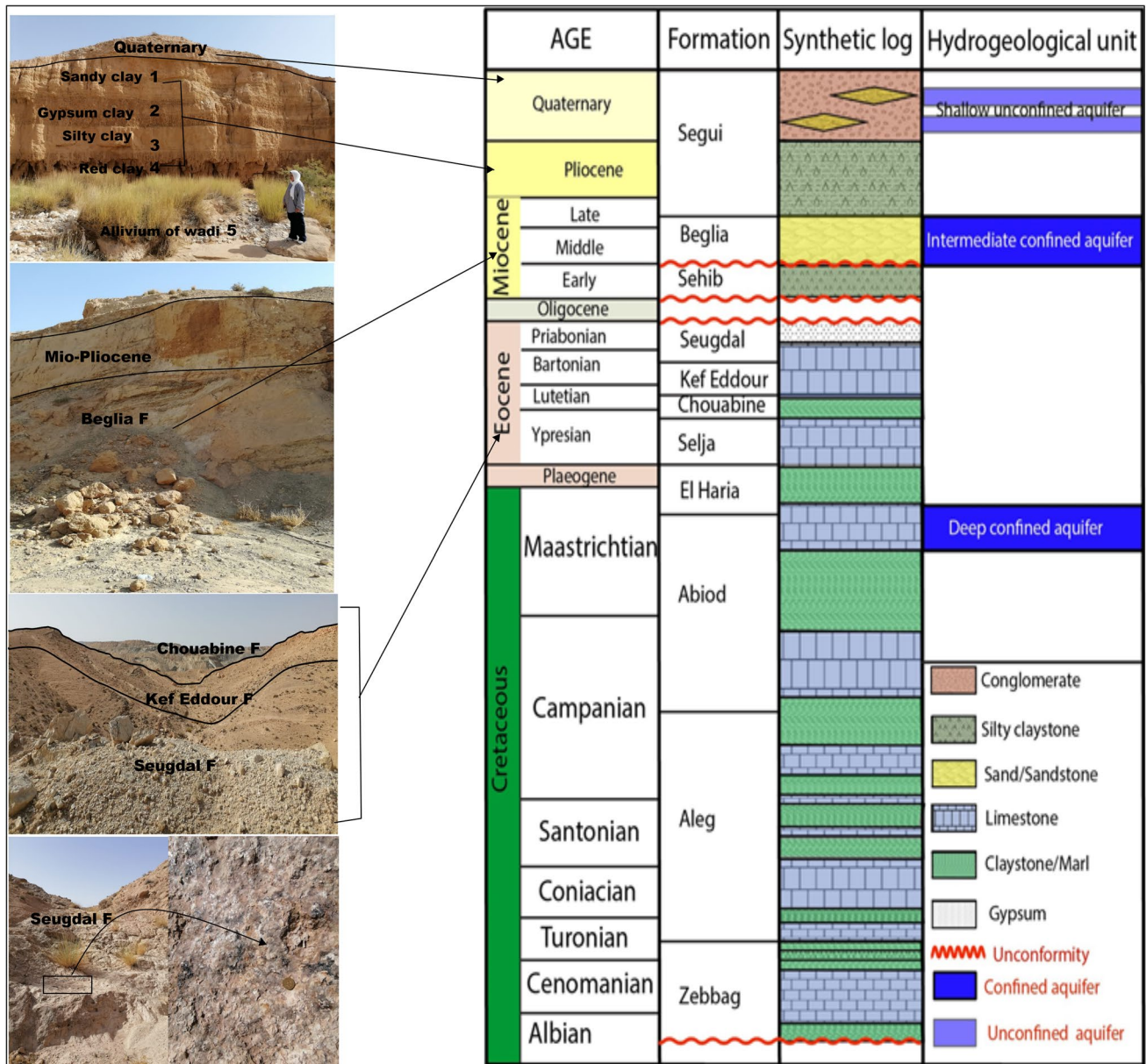


Fig. 5 Hydro-stratigraphic column of the Garâat Douza-Tabeditt basin (Mhamdi et al. 2022) with some field photographs

and that is theoretically calculated under the same conditions (identical electrode geometry and injected current intensity) for a homogeneous resistivity field 1 (Marescot et al. 2008).

As part of this study, five electrical resistivity tomography (ERT) profiles are obtained using a Winner array to search for an essentially horizontal structure, which is then used to determine the salinization extent. The Winner array used an SYSCAL Pro resistivimeter (IRIS-Instruments-France), which measures the apparent resistivity, and an acquisition unit with RES2DINV switching software. The coordinates (X and Y) of each profile's the first and last electrode are taken using a hand GPS unit (Fig. 7).

Results

Hydrogeology

The piezometric map of the Pliocene–Quaternary ground-water table of 2019 shows the variation of the piezometric levels between 374 and 344 m deep (Fig. 8).

There are three main directions of water flow, two of which tend to supply the El Berka region, directed respectively west–east and northeast–southwest (from Tabeditt wadi (valley) and Moulares to the El Berka plain). A direction northwest–southeast tends to supply

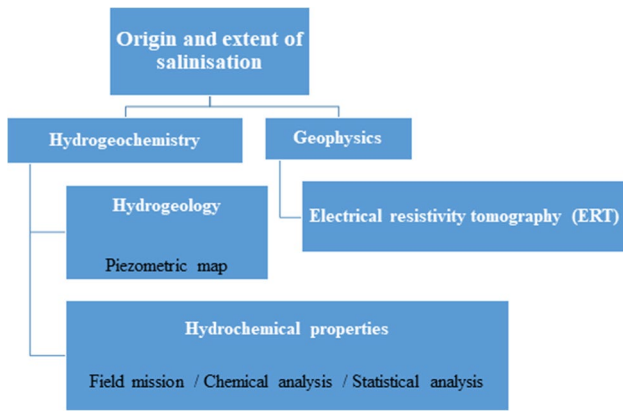
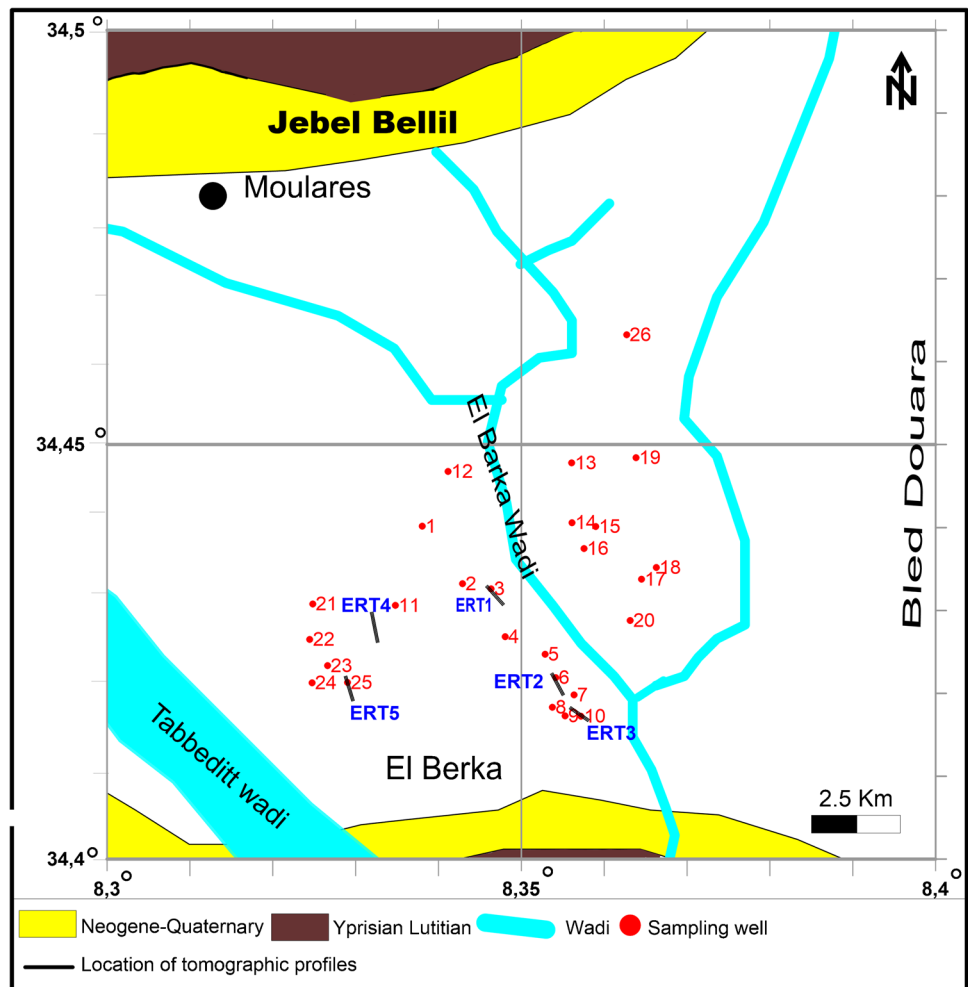


Fig. 6 Flowchart of the methodological approach adopted in this work

El Berka wadi (valley). These new data have shown that the water table in the Pliocene–Quaternary aquifer of El Berka has dropped by 5 m compared with the data from the piezometric map published by Gouasmia (2008).

Fig. 7 Localization map of water wells and ERT profiles



Hydrochemical properties

The reported pH ranges from 7.61 to 8.39, and the conductivity ranges from 1.87 to 16.94 ms/cm. The salinity map (Fig. 9) shows the spatial variation of the dry water residue from 2 to 13 g/l.

Salinity tends to increase in the direction of the flow of the water. In this direction, water is increasingly enriched by other elements that contribute to high salinity in the region.

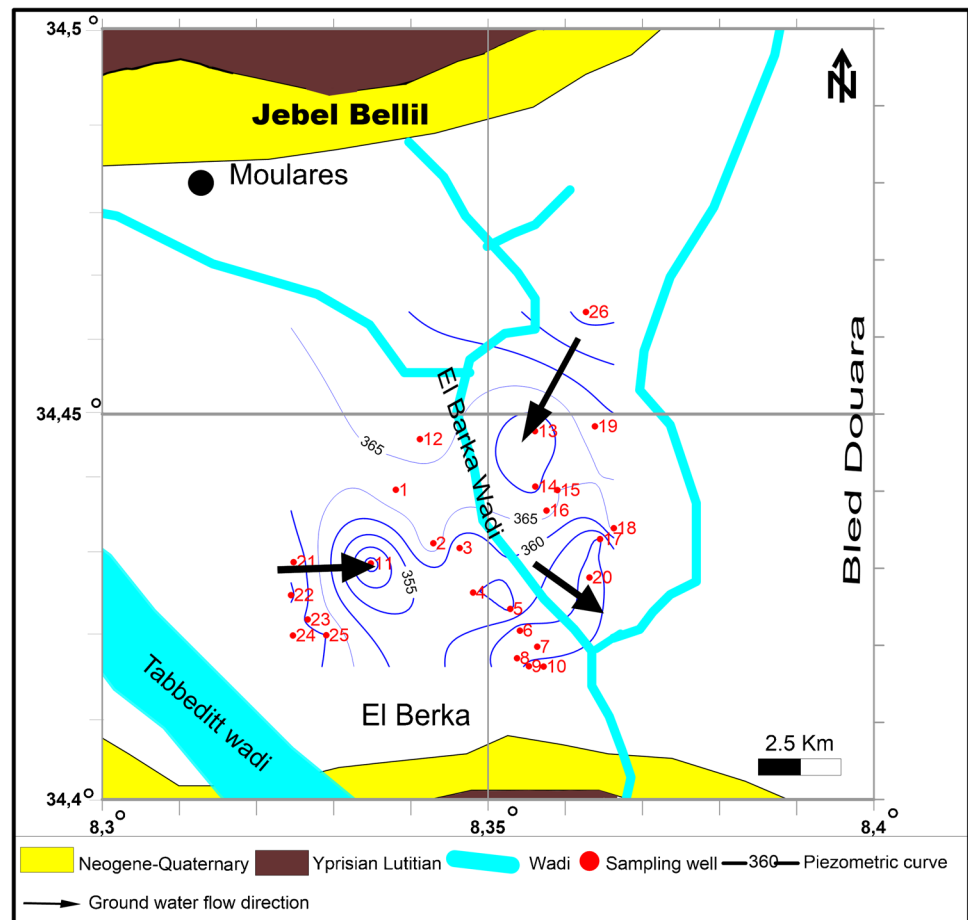
The distribution maps of the major elements (Fig. 10) have shown that the chemical composition of the Pliocene–Quaternary groundwater is chemically dominated by Ca cations and Cl anions. The relative abundance is in the order of Na > Ca > Mg for the cations and SO₄ > Cl > HCO₃ for the anions. Sodium is always present in natural waters in varying proportions. It originates from the leaching of NaCl-rich formations (halite).

Observation of the Na distribution map indicates sodium concentrations (250 to 1200 mg/l) (Fig. 10a), with high concentrations in the southeast, and calcium levels (120 to 580 mg/l) (Fig. 10b), with high concentrations in the

Table 1 In situ measurement geochemical data and saturation indexes of ground waters

Well N°	In situ measurements				Elemental composition										Saturation indexes (SI)					
	T (°C)	PH	Ec (ms/cm)	S (g/l)	TDS (mg/l)	Ca ²⁺ (mg/l)	Mg ²⁺ (mg/l)	Na ⁺ (mg/l)	K ⁺ (mg/l)	Cl ⁻ (mg/l)	HCO ₃ (mg/l)	SO ₄ ²⁻ (mg/l)	NO ₃ ⁻ (mg/l)	Anhy-drite	Arago-nite	Calcite	Dolo-mite	Gyp-seum	Halite	
1	22	8.39	4.62	3.55	2771.695	266	70.48	504.88	15.01	631.77	62.525	1214.21	6.82	-0.66	0.6	0.74	1.24	-0.44	-5.17	
2	19	7.71	6.55	3.76	4180.95	389	94.8	762.40	27.01	824.57	439.2	1632.81	11.16	-0.49	0.9	1.04	1.8	-0.27	-4.9	
3	21	8.01	5.38	5.93	3237.67	333	71.269	565.74	19.50	613.98	97.6	1527.91	8.68	-0.52	0.5	0.64	0.94	-0.3	-5.15	
4	21	8.24	13.88	5.68	5201.22	500	169.18	919.62	27.11	1575	42.7	1936.61	31	-0.32	0.45	0.6	1.06	-0.17	-4.56	
5	21	7.79	7.04	5.34	4082.39	464	131.47	614.07	20.62	875	282.3	1686.25	8.68	-0.42	0.86	1	1.79	-0.2	-4.97	
6	21	7.94	12.58	10.79	5332.19	458	145.04	1077.11	27.01	1575	82.35	1958.38	9.3	-0.04	0.42	0.57	0.97	-0.2	-4.49	
7	19	7.76	15.72	9.98	5781.97	540	179.68	1014.78	26.52	1400	516.25	2092.96	11.78	-0.35	1.1	1.24	2.34	-0.13	-4.57	
8	21	8.32	9.13	12.64	4554.04	400	131.63	889.84	16.32	1435	56.45	1613.02	11.78	-0.5	0.58	0.73	1.31	-0.29	-4.6	
9	21	7.8	10.32	6.8	5122.08	406	130.43	1085.47	17.28	1645	36.6	1795.10	6.2	-0.48	-0.1	0.04	-0.07	-0.26	-4.47	
10	21	8.11	16.94	7.89	5507.444	380	146.60	1152.46	66.01	1435	213.48	2105.83	8.06	-0.47	0.9	1.05	2.02	-0.25	-4.51	
11	21	8.01	4.12	3.18	3751.45	328	71.47	786.16	20.48	1053.5	42.7	1439.84	9.3	-0.57	0.13	0.27	0.22	-0.35	-4.78	
12	21	7.7	6.6	5.22	3902.22	400	107.16	653.27	27.11	738.5	153.72	1811.92	10.54	-0.43	0.44	0.58	0.93	-0.21	-5.02	
13	21	8.21	5.04	2.5	2535.14	244	69.39	453.81	17.20	562.45	89.95	1086.56	11.78	-0.72	0.57	0.72	1.23	-0.5	-5.26	
14	21	7.65	4.35	3.23	3551.62	331	82.43	659.82	25.73	754.95	222.45	1466.56	8.68	-0.56	0.5	0.65	1.02	-0.34	-5	
15	21	7.91	6.41	4.89	3524.93	366	71.06	650.24	27.11	822.5	71.7	1500.20	16.12	-0.51	0.3	0.45	0.52	-0.29	-4.97	
16	21	8.24	5.93	4.25	4133.98	400	130.69	698.70	27.11	948.85	395	1519.99	13.64	-0.51	1.36	1.51	2.87	-0.3	-4.88	
17	19	8.13	11.97	9.3	6039.74	570	134.60	1185.49	26.72	1963.5	102.2	2050.41	6.82	-0.33	0.77	0.91	1.54	-0.12	-4.36	
18	21	7.77	1.58	4.01	3823.23	300	129.75	761.74	27.11	1266.65	74.75	1250.83	12.4	-0.68	0.12	0.26	0.5	-0.46	-4.71	
19	21	8.02	6.91	5.12	4575.81	455	132.52	806.04	27.01	1177.4	252.85	1711.97	13.02	-0.44	1.01	1.15	2.1	-0.22	-4.73	
20	21	7.63	10.44	8.08	5203.75	459	132.67	1017.48	26.91	1410.5	193.35	1956.40	7.44	-0.41	0.5	0.64	1.08	-0.19	-4.56	
21	21	7.8	3.32	2.45	2379.45	271	129.70	263.97	7.37	473.58	51.25	1167.70	14.88	-0.67	-0.01	0.13	0.27	-0.45	-5.57	
22	21	8	2.17	1.56	2120.28	155	67.35	396.97	4.15	280.7	130.9	1079.63	5.58	-0.88	0.36	0.5	0.97	-0.66	-5.61	
23	21	7.96	1.87	3.42	1942.91	150	56.34	355.76	3.75	247.8	88.45	1032.13	8.68	-0.89	0.15	0.29	0.49	-0.67	-5.71	
24	21	8.09	3.32	3.06	2533.44	244	68.974	432.83	5.16	386.75	83.9	1306.25	5.58	-0.66	0.41	0.55	0.89	-0.44	-5.45	
25	21	8.08	1.58	3.25	1983.8	130	56.34	395.37	3.09	245.7	187.6	959.5	6.2	-0.97	0.53	0.86	1.32	-0.75	-5.67	
26	21	7.61	4.43	9.3	3129.55	366	70.43	517.45	18.76	719.95	68.6	1359.68	8.68	-0.52	0.02	0.16	-0.06	-0.3	-5.11	

Fig. 8 Piezometric map of the study area



entire region. It is mainly due to the dissolution of carbonate (CaCO_3) and evaporate (gypsum or anhydrite). Magnesium concentrations vary between 55 and 180 mg/l (Fig. 10c). The higher levels are recorded in the southeastern part of our study area. Cations (Mg^{2+} and Ca^{2+}) come from carbonate dissolution formations rich in magnesium (dolomites). The high magnesium concentrations potentially result from the leaching of carbonates or evaporate of the Lutetian age Seugdala formation. Sulfate contents vary between 950 and 2150 mg/l (Fig. 10d). Their concentration is very high in all sides of El Berka Wadi. The high sulfate concentration is due to the simultaneous dissolution of anhydrite and gypsum from evaporative formations. Chloride concentrations are between 200 and 2000 mg/l (Fig. 10e), with a remarkable increase in the southeastern part of the study area.

The concentration of bicarbonates varies from 0 to 500 mg/l (Fig. 10f). This seems to be due to the dissolution of carbonate minerals. Besides, nitrate levels range between 5 and 31 mg/l (Fig. 10g). In addition, nitrate reflects the application of fertilizers during agricultural activities.

The representation of water points on the triangular Piper diagram for the El Berka region shows a trend towards the sodium pole in the sub-triangle cations. In contrast, the

anions have shown a dominance of sulfate. The diagram shows sulfate chloride sodium and calcium facies (Fig. 11a).

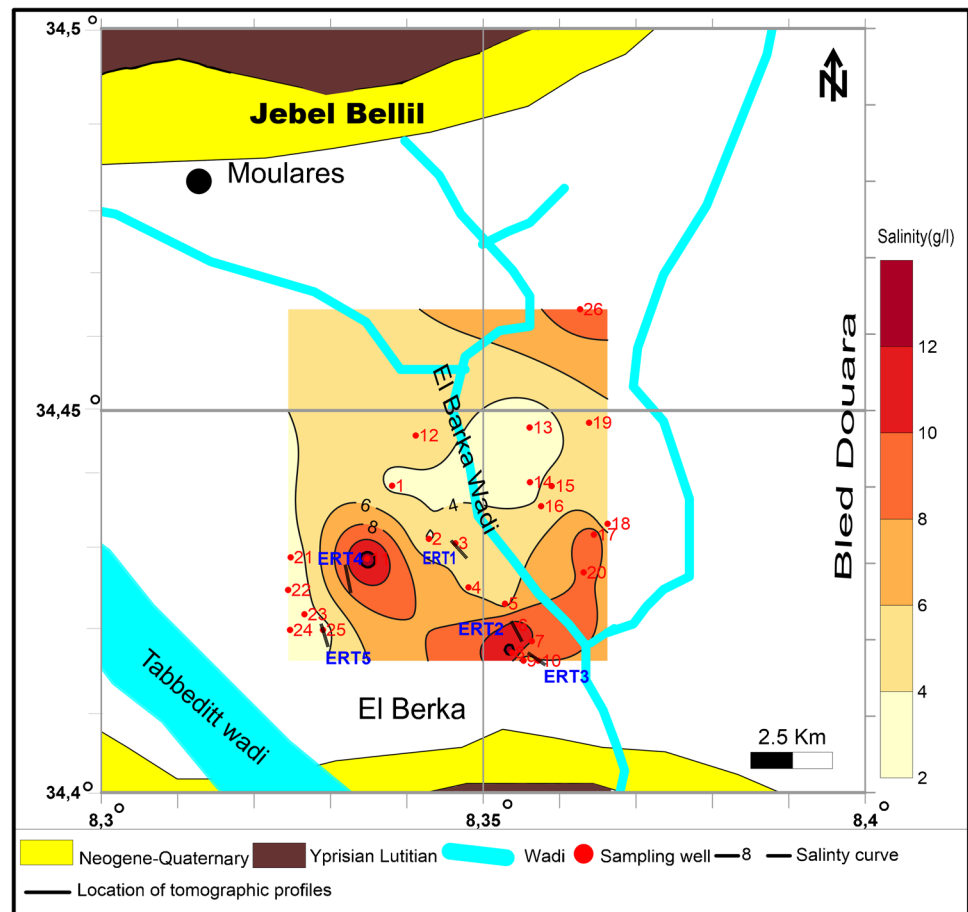
In addition, the Schoeller-Berkaloff diagram (Fig. 11b) shows that most samples are characterized by high sulfate, chloride, sodium, and calcium contents. So, according to the Piper and Schoeller-Berkaloff diagrams, salinity is generated by the dissolution of the sulfate, chloride, sodium, and calcium minerals.

The anion/ Σ anions and cation/ Σ cation correlations (Fig. 12) show good correlations for sodium ($R^2 = 0.954$) and calcium ($R^2 = 0.817$). Similarly, sulfate shows a good correlation as a function of the sum of anions ($R^2 = 0.916$) and chloride ($R^2 = 0.887$). Therefore, this indicates that Na, Ca, SO_4 , and Cl play an essential role in the acquisition of the salinity of the groundwater.

The examination of the Na^+ versus Cl^- plot has shown a good correlation between these two elements (Fig. 13a). In addition, the proportional evolution of the saturation index (SI) for halite and the sum of ($\text{Na} + \text{Cl}$) (Fig. 14a) strongly suggests that dissolution of halite seems to be a source for the chloride-sodium composition in the aquifer.

The excellent correlation between Ca^{2+} and SO_4^{2-} ($R^2 = 0.829$) (Fig. 13b) points to a gypsum and/or

Fig. 9 Salinity map of the study area



anhydrite source. This is further confirmed by the parabolic and proportional evolution between SI and the sum of the ions (Ca^{2+} and SO_4^{2-}), resulting from the possible dissolution of these two minerals (Fig. 14b and c).

The saturation indices for all the samples (Table 1) have values close to zero and are slightly positive for aragonite, dolomite, and calcite. Indicating that the water is saturated concerning to these minerals and is negative for the evaporate minerals (anhydrite, gypsum, halite), which shows that the investigated waters are under-saturated relative to these minerals. This suggests that the dissolution of the latter is quite likely. Thus, we can conclude that the mineralization of the El Berka Pliocene–Quaternary groundwater can be due to the dissolution of evaporates.

Statistical analysis

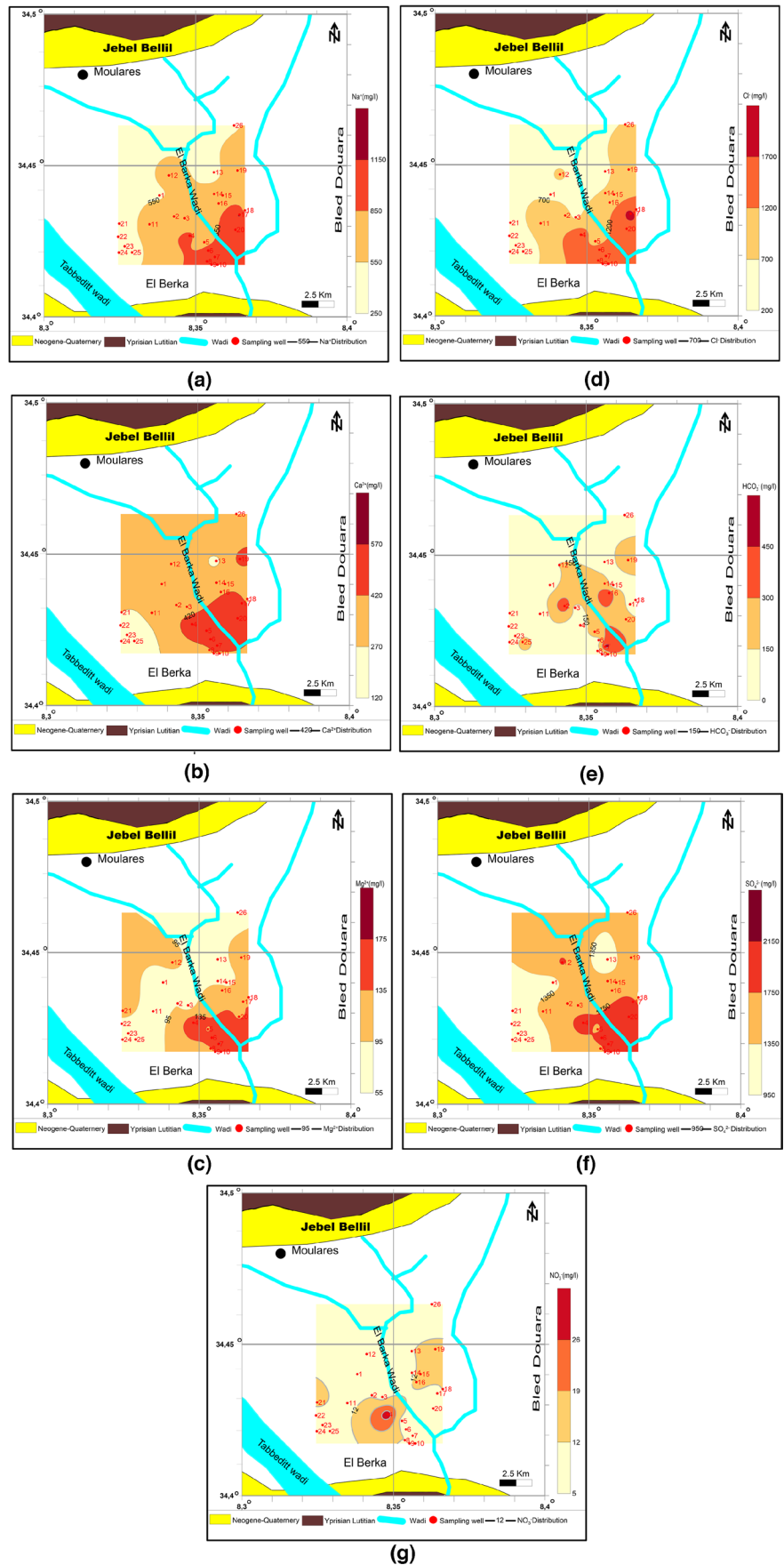
The statistical analysis has enabled us to determine the elements responsible for groundwater mineralization. In this study, both the principal component analysis (ACP) and hierarchical cluster analysis (HCA) have been performed to constrain better the interpretation of chemical data (pH, salinity, Ca^{2+} , Mg^{2+} , Na^+ , K^+ , HCO_3^- , Cl^- , SO_4^{2-} , and

NO_3^-). Analysis of the correlation matrix (Table 2) shows that sodium, sulfates, chloride, calcium, and magnesium are highly correlated with TDS. The correlation coefficients are respectively 0.965, 0.954, 0.949, 0.917, and 0.832, which indicate the contribution of these elements in the mineralization of the groundwater of El Berka region.

The main components analysis is conducted on ten physico-chemical parameters from the analysis of water sampled over the entire study area (Table 2, Fig. 15a,b,c). The eigenvalues and the percentage of variance explained by each vector are listed in Table 3. We highlight the associations between the different variables and the possible existence of subpopulations. A correlation matrix of 10 parameters shows fascinating solid and positive correlations of the waters of the Pliocene–Quaternary (Table 3) showing that the first axis (F1) is around 60.05% of the total variance and the second 13.78% (F2).

The sum of these two principal Eigenvalues equals 73.83% (Table 2). It is correlated with high loads of TDS, Ca^{2+} , Mg^{2+} , Na^+ , K^+ , Cl^- , and SO_4^{2-} (Fig. 15a). Therefore, it shows the natural processes of mineralization of groundwater. The spatial graphical representation of the statistical units of factorial plane F1-F2 (Fig. 15b) shows a competition, according to the

Fig. 10 Spatial distribution maps of the main major elements [a Ca^{2+} ; b Mg^{2+} ; c Na^+ ; d Cl^- ; e HCO_3^- ; f SO_4^{2-} ; g NO_3^-]



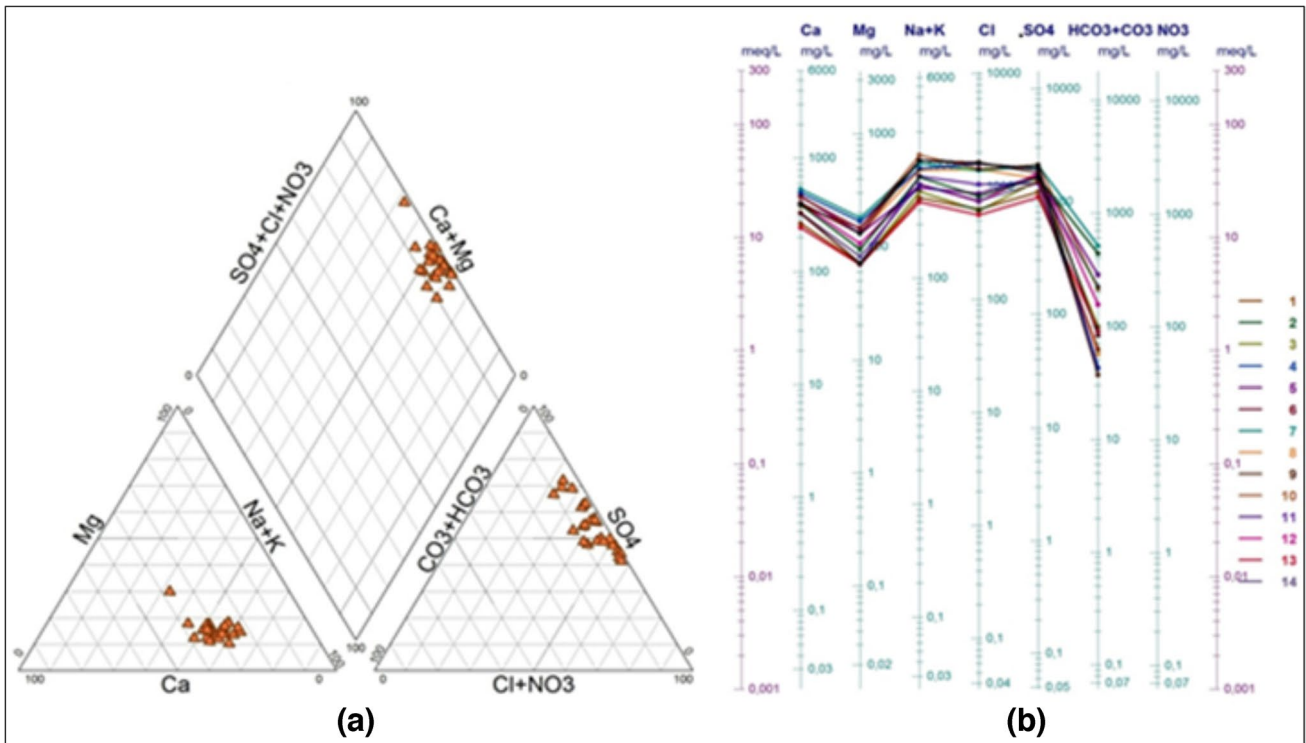
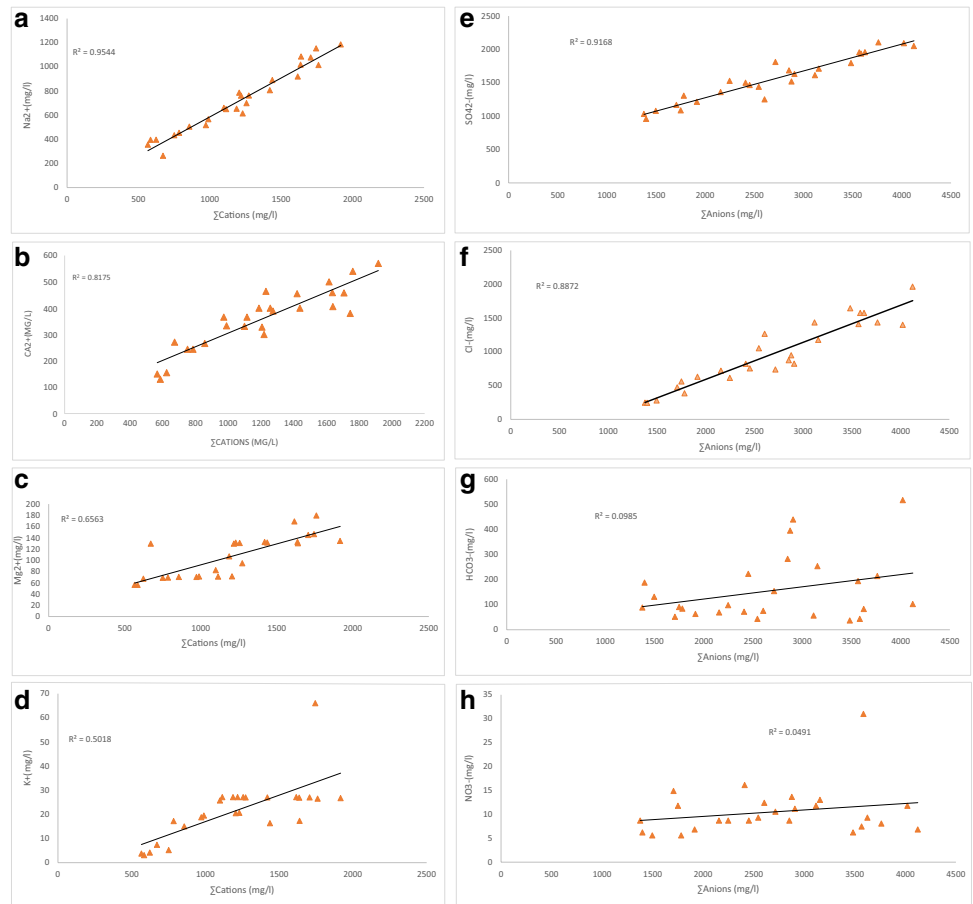


Fig. 11 a Piper diagram of the groundwater samples, b Schoeller Berkaloff diagram of the groundwater samples

Fig. 12 Correlations of major element contents with the sums of cations and anions



F1 axis, between chlorinated and sodium sulfate waters on the positive side of the axis and calcium bicarbonate waters on the negative side. Water from calcareous and marly carbonate aquifers is low salinity, while water from aquifers containing evaporative saliferous or gypsum rocks is more saline. This salinity is remarkable in the samples going from upstream to downstream of the basin, confirming the hypothesis of contamination of the waters by the phenomenon of dissolution.

The hierarchical upward classification shows groundwater samples are subdivided into three groups (Fig. 15c). Group (C1) consists of 7 wells. This water group includes, on the one hand, the least mineralized waters. It is characterized by low TDS and low concentrations of Ca^{2+} , Mg^{2+} , Na^+ , HCO_3^- , Cl^- , and SO_4^{2-} compared to groups 2 (contains 12 wells) and 3 (includes 7 wells) (Table 4) of medium to high

concentration. They are mainly characterized by strongly mineralized waters or influenced by the water–rock interaction and the process of hydrolysis in acquiring the mineralization of the waters during their infiltration.

Tomography results (ERT)

The choice of the geo-electrical method is motivated by the satisfactory results obtained for the characterization of surficial aquifers in Tunisia (Abdelkader et al. 2018; Mhamdi et al. 2006; 2015; 2013; Gouasmia et al. 2018, Moussaoui et al. 2018). The ERT profiles were realized in a parcel between Wadi El Berka and Wadi Tabeditt (Fig. 7) to determine the salinization extent. The obtained results allow classifying the ERT profiles in two groups (Fig. 16).

Fig. 13 Bivariate diagrams between major elements: **a** Na^+/Cl^- ; **b** $\text{Ca}^{2+}/\text{SO}_4^{2-}$

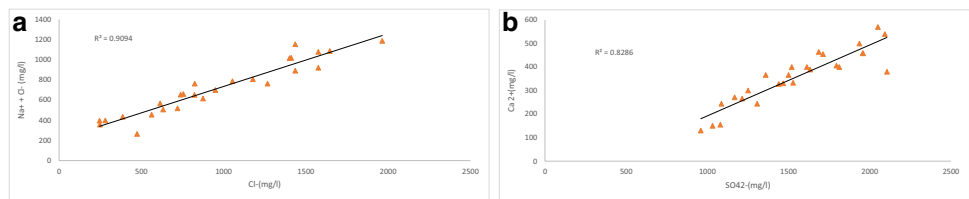


Fig. 14 Mineral saturation indexes versus representative species relationship: **a** SI halite/ ($\text{Na}^+ + \text{Cl}^-$), **b** SI gypsum/ ($\text{Ca}^{2+} + \text{SO}_4^{2-}$), **c** SI anhydrite/ ($\text{Ca}^{2+} + \text{SO}_4^{2-}$)

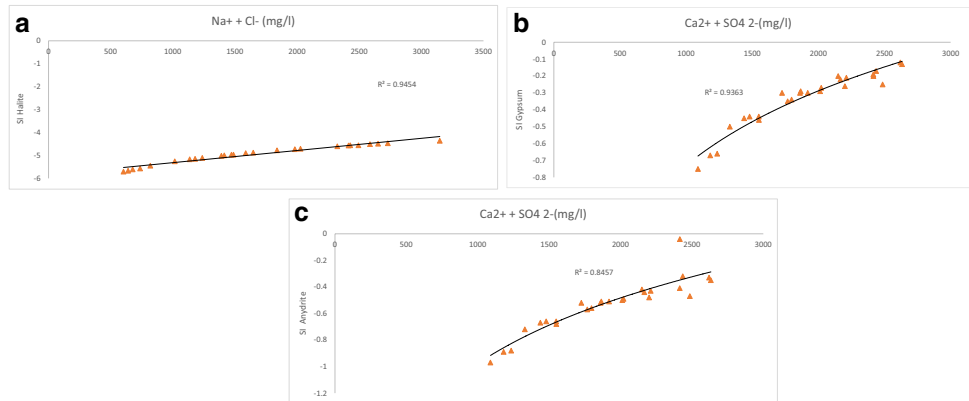


Table 2 Correlation matrix of the groundwater samples from El Berka region

Variables	PH	TDS (mg/l)	Ca (mg/l)	Mg (mg/l)	Na (mg/l)	K (mg/l)	Cl (mg/l)	HCO3 (mg/l)	SO4 (mg/l)	NO3 (mg/l)
PH	1									
TDS	-0.075	1								
Ca (mg/l)	-0.148	0.917	1							
Mg (mg/l)	-0.051	0.832	0.785	1						
Na (mg/l)	-0.022	0.965	0.800	0.723	1					
K (mg/l)	-0.061	0.704	0.580	0.535	0.700	1				
Cl (mg/l)	0.028	0.949	0.840	0.793	0.954	0.603	1			
HCO3 (mg/l)	-0.244	0.293	0.319	0.321	0.181	0.298	0.045	1		
SO4 (mg/l)	-0.142	0.954	0.910	0.780	0.893	0.719	0.838	0.315	1	
NO3 (mg/l)	0.174	0.215	0.322	0.425	0.097	0.188	0.239	-0.035	0.195	1

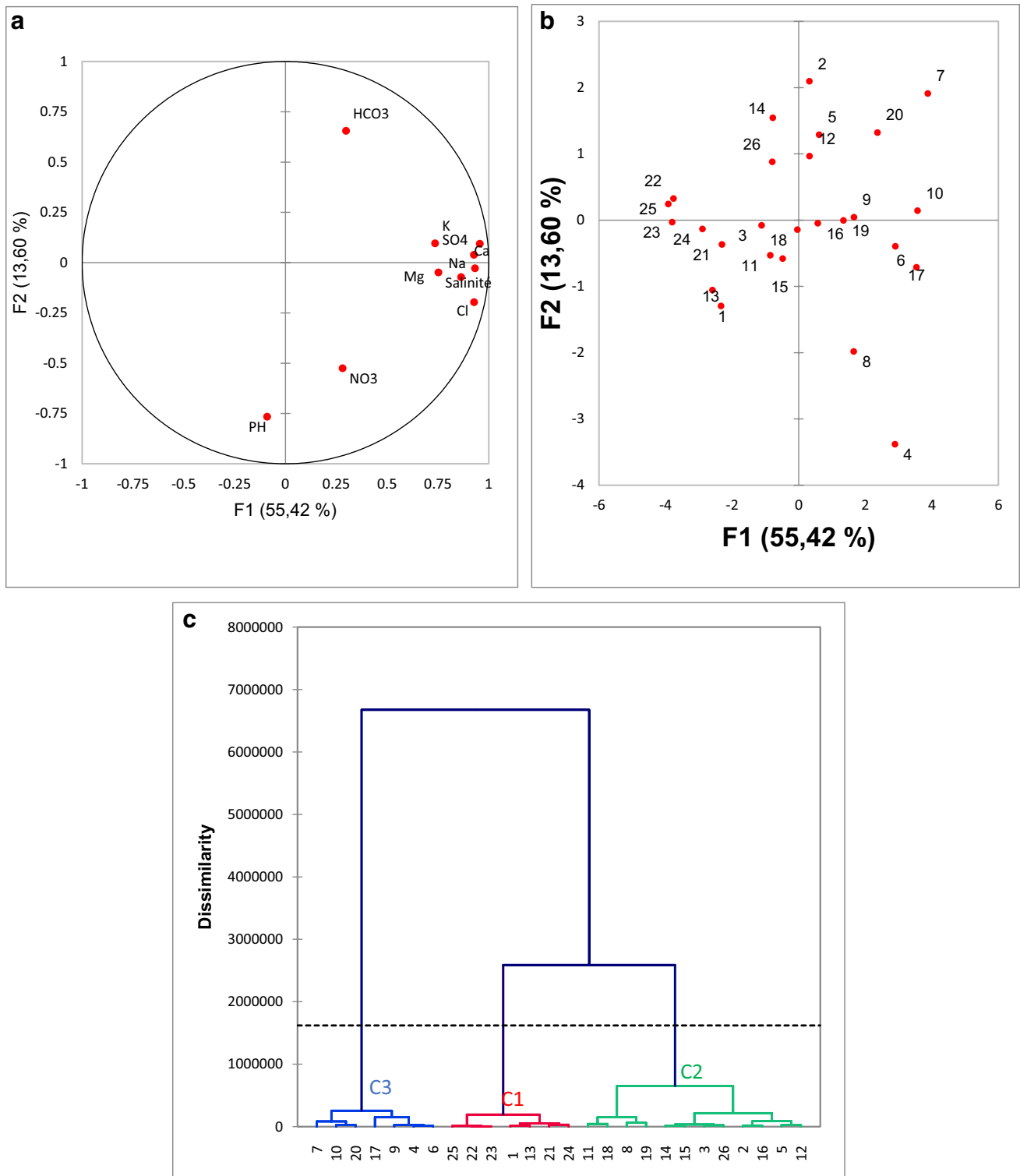


Fig. 15 Statistical analysis [a plot of principal component analysis of variables, b projection of groundwater samples onto the factorial plane (F1/F2), c hierarchical cluster analysis (HCA): dendrogram of the groundwater samples from El Berka region]

A high resistivity occurred in profiles 1 and 5 (more than 16Ω.m), which can be attributed to low groundwater salinity (less than 6 g/l). Conversely, low resistivity observed in

profiles 2, 3, and 4 (less than 10Ω.m) seems to be related to high groundwater salinity (more than 7.5 g/l).

Table 3 The principal component analysis results

Axis component	F1	F2
Owen value	6005	1358
Variability (%)	60,046	13,585
Cumulative%	60,046	73,631

The ERT results confirm and complete the results obtained by geochemical interpretation and in particular the salinity map (Fig. 7). The tomographic profiles show the same trend as the salinity map, indicating that the Pliocene–Quaternary groundwater of the El Berka region contains a low electrical resistivity zone in the center with a relatively high resistivity approximately at the mountainous and wadi Tabeditt areas.

Discussions

The electrical resistivity tomography data allows the identification of the succession of the following water tables:

A highly resistant superficial layer can reach a thickness of 7 m, corresponding to conglomerates, pebbles, and alluvium. An intermediate level of low resistivity with sands and clays that are saturated with salt water.

A lower relatively resistant level that may contain water of better quality than the intermediate level.

The characterization of the aquifer units was achieved by integrating geophysical data (ERT) and well data. The combination of the electrical resistivity tomography and geochemistry data shows that the salt concentration in the waters of the Pliocene–Quaternary aquifer of the El Berka region is the result of the following three successive processes:

Process A (ancient state of the El Berka basin): Significant amounts of rainfall on the Moulares and Metlaoui mountain ranges, specifically Jebel Billil in the north and Jebel Alima in the south (Fig. 2). These rainwaters are enriched in salts by leaching of evaporate rocks from the evaporate Seugdai formation. As this water then flowed towards El Berka, some of the water seeped into the groundwater, and the rest of the water evaporated and accumulated salts at the surface (Fig. 17a).

Process B (intermediate state of the El Berka basin): The arid climate of Southern Tunisia is the driving force behind evaporation. It is from these sources of water that the salts in solution get concentrated and then precipitate forming evaporated rocks such as gypsum, anhydrite, and halite from secondary sedimentary brines (Fig. 17b).

Process C (current state of the El Berka basin): During the diagenesis of the saline rocks, part of them will leach again into the groundwater, which will become increasingly concentrated in salts (Fig. 17c). The current state of the models shows an evolution in time and space of the aquifer levels. It is believed that all available results were combined to explain the salinization process in the study area.

The existence of secondary evaporates in the superficial sediment is the result of dissolution rather than the evaporation of the primary evaporates (Bryant et al. 1994). So, the evaporative history is the result of a succession of very slow geological and geochemical events and the result of agricultural fertilizers (irrigation). Dissolution of evaporate rocks is known to be an agent of groundwater salinization in Southern Tunisia (Mascle et al. 1986; Bryant et al. 1994; Tarki et al. 2012; Kraiem et al. 2014; Mhamdi et al. 2015).

This happens especially when the ground has large volumes of evaporate rocks and/or when recharge water drains evaporated rocks and dissolves considerable quantities of salt following the chemistry of the water inflow in the Chott el Djerid (Bryant et al. 1994). Recharge also occurs via the leakage of upward flow from the deep aquifer (Houcine et al. 2014). The salts can be mobilized by lateral infiltration. Aquifer salinization may also occur due to saline water input from the underlying aquifer (Zouari et al. 2003; Krimissa et al. 2004), from contamination by hyper-saline aquifers and ascent of high salinity deep waters along faults (Zouari et al. 2006; Kraiem et al. 2015), and from Sabkha (chotts, salt lakes) at the surface (Mhamdi et al. 2006).

In Southern Tunisia which is characterized by intense evaporation, rock–water interaction and local irrigation practices such as submersion irrigation and drainage basin are the main processes that affect groundwater composition (Moussaoui et al. 2018; Agoubi et al. 2013; Kraiem et al. 2012). Our research shows that it is also the case in our study area. It is worth mentioning that the same phenomenon has been observed in other regions of Southern Tunisia such as Gareet Douza (Moussaoui et al. 2018), the Jeffara aquifer in the southeast (Agoubi et al. 2013), as well as the in the oasis shallow aquifers of Nefzaoua region in Southwest Tunisia (Kraiem et al. 2012). The origin of water mineralization in central Tunisia is most probably related to the dissolution of evaporate minerals and the exchange of cations, as in the case of the Chougafiya basin (Farid et al. 2012). On the other hand, water–rock interaction processes and the backflow of irrigation water have led to high concentrations of nitrates in groundwater, especially in agricultural areas, due to the excessive use of fertilizers in the open aquifers of BouHafna-Haffouz (El Mejri et al. 2018). The groundwater of the Sidi El Hani basin (central-eastern Tunisia) is

Table 4 Mean values of the chemical constituents of groundwater clusters

Cluster	PH	TDS (mg/l)	Ca (mg/l)	Mg (mg/l)	Na (mg/l)	K (mg/l)	Cl (mg/l)	HCO3 (mg/l)	SO4 (mg/l)	NO3 (mg/l)
1	8076	2,323,816	208,571	74,081	400,513	7961	404,107	99,225	1,120,854	8503
2	7895	3,870,653	377,667	102,056	697,123	23,656	935,904	179,777	1,543,415	11,057
3	7944	5,455,485	473,286	148,314	1,064,630	31,080	1,572,000	169,562	1,985,099	11,514

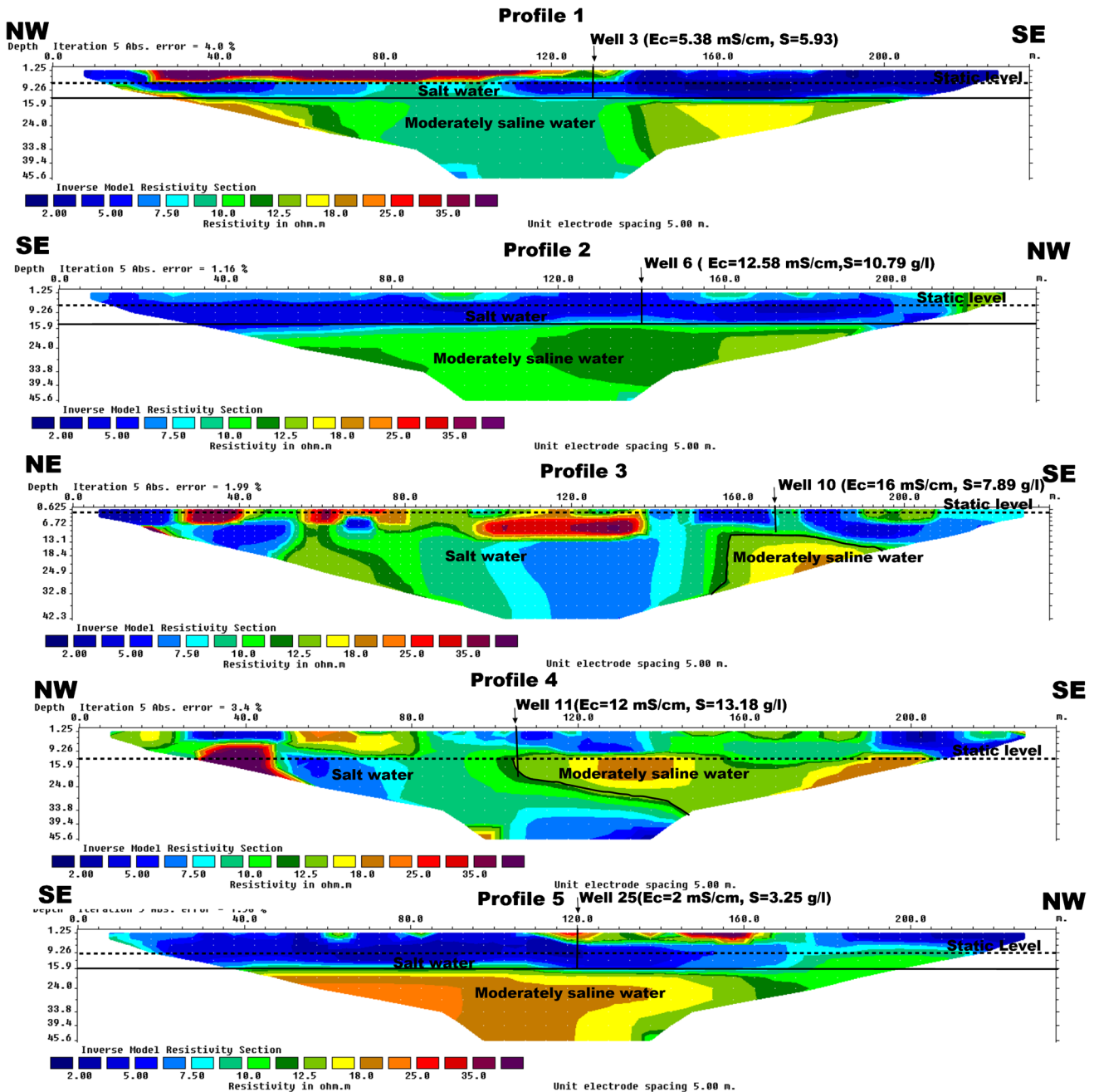


Fig. 16 Profiles of electrical resistivity tomography

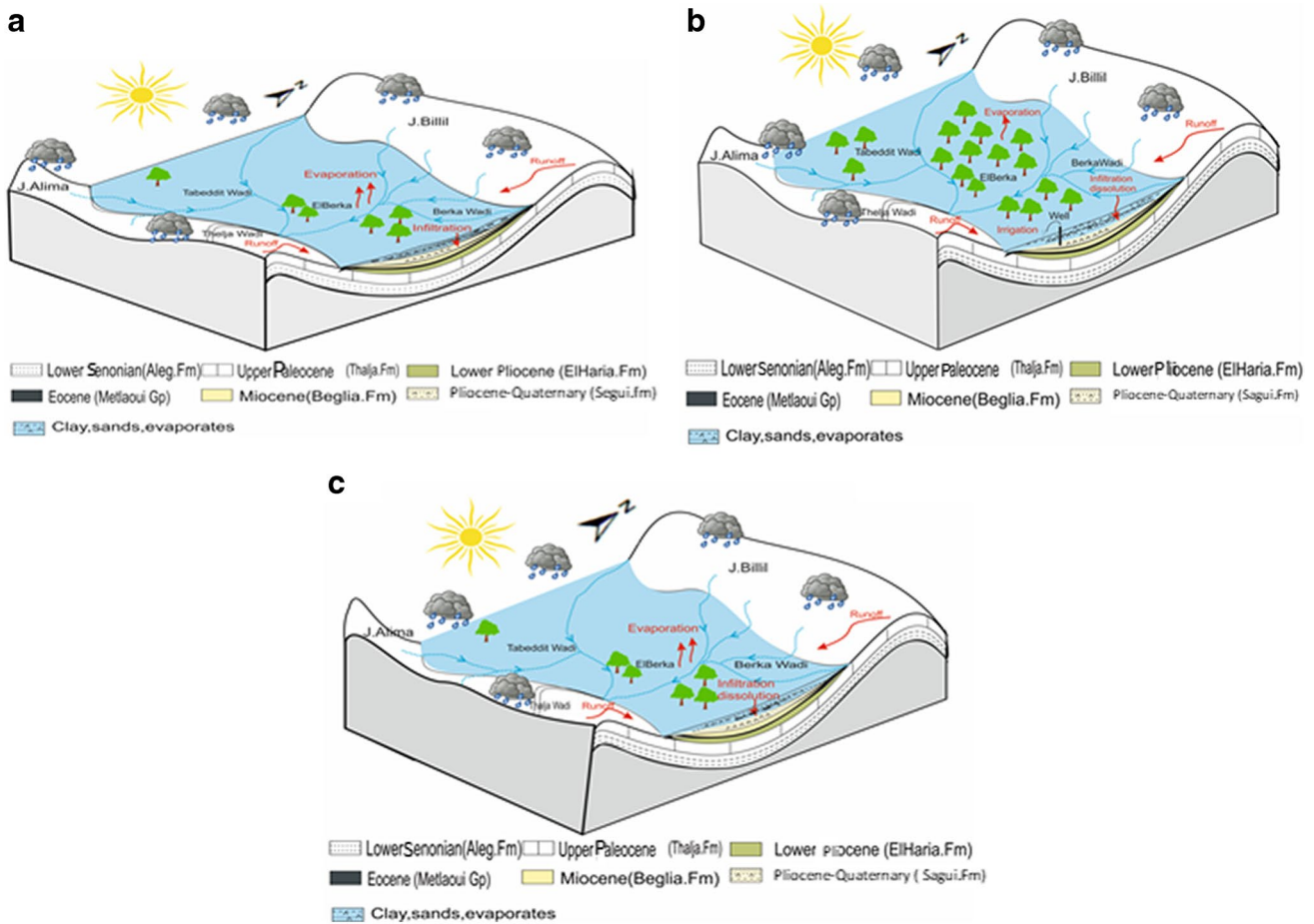


Fig. 17 Successive processes of the salt concentration in the waters of the Pliocene–Quaternary aquifer of the El Berka region **a** (Processes A), the ancient state of the El Berka basin; **b** (Processes B), the inter-

mediate state of the El Berka basin; **c** (Processes C), the current state of the El Berka basin]

affected by the dissolution of halite, gypsum, and anhydrite with simultaneous precipitation of calcite and dolomite in association with ion exchange and inverse ion exchange with clay minerals (Lotfi et al. 2018).

Northern Tunisia is affected by seawater intrusion, just like in the region of Maâmoura (Chabaane et al. 2018) and the coastal aquifer of Nabeul-Hammamet (Trabelsi et al. 2016). The causes of salinization differ from one country to another. In the Wadi Nador coastal aquifer (Tipaza, Algeria), intensive good pumping, hydraulic connection to the sea, and high porosity of the Pliocene–Quaternary aquifer are the leading causes of groundwater salinization (Bouderbala and Remini 2014). The salinization in the Hassi Miloud area, Algeria, is related to the combined effects of irrigation and upwelling from the saturated zone (Semar et al. 2019). Dissolution of halite, carbonate weathering, and mixing of seawater are the main factors controlling groundwater in the Aseer region of Saudi Arabia (Mallick et al. 2018). Chemical alteration of rock-forming minerals controlled shallow groundwater in the Dongsheng Coal Basin

in the Ordos Basin, China (Li et al. 2013). In coastal aquifers in Portugal, human-induced water quality degradation intensifies salinity directly through pollution or indirectly through agricultural activity over-pumping that leads then to the invasion of saline groundwater in freshwater aquifers (Carreira et al. 2014). In Egypt, for instance, the salinity of groundwater results from the precipitation of calcite, dissolution of dolomite and gypsum, as well as the exchange of sodium in groundwater with calcium and magnesium in the aquifer matrix along the groundwater flow path in the central part of the country (Mosaad and Kehew 2019), while northwest of the Nile Delta groundwater quality in shallow aquifers is controlled mainly by the dissolution of evaporate minerals and seawater intrusion, contamination of nitrogen compounds by anthropogenic activities, agricultural fertilizers, and domestic drainage water (Masoud 2014). In the coastal aquifers of Morocco, water salinity can be induced by marine intrusion due to the absence of red clays, favoring the penetration of seawater and the decrease in the recharge rate of aquifers caused by the decrease in rainfall under the

effect of climate change. Moreover, groundwater chemistry is also influenced by water–rock interaction and anthropogenic activities (application of fertilizers, septic tank use) in the upstream area (Najib et al. 2017; Fadili et al. 2017; Ouhamdouch et al. 2019).

Conclusion

This study has aimed at integrating hydrochemical and geophysical (ERT) data for the study of the salinization of the Pliocene–Quaternary aquifer in the zone of El Berka (Southwest Tunisia). The hydro-geochemical analysis made it possible to determine that the high salinization of groundwater in the Pliocene–Quaternary sands resulted from the mineralization of waters from the mountain ranges and the dissolution of minerals (evaporates) existing on the plain. The ERT profiles allow to determine the extension of salt-water levels. Generally, evaporation enrichment is achieved by trapping groundwater in low-permeability materials. The high evaporation rate is combined with irrigation and induces salt precipitation and accumulation in the unsaturated zone. It should also be noted that water infiltration dissolves the rocks by rainfall.

Acknowledgements The authors gratefully acknowledge the contribution of the staff members of the Faculty of Science of Gafsa for their help during fieldwork. We also thank the technical staff of the Hydrological Laboratory of the Gafsa Phosphate Company and the Geodynamic Service and Mineral Resources of the Department of Earth Sciences at the Royal Museum of Central Africa (Tervuren, Belgium) for their help.

Declarations

Conflict of Interest The authors declare that they have no competing interests.

References

- Abdelkader M, Gouasmia M, Dhahri F, Lahmadi M (2021) Soussi M (2018) Integrated geoelectrical and hydrogeological study of Garaat Sened area, west-central Tunisia. *Arab J Geosci* 14:66. <https://doi.org/10.1007/s12517-021-06486-9>
- Agoubi B, Kharroubi A, Abichou T, Abida H (2013) Hydrochemical and geoelectrical investigation of Marine Jeffara Aquifer, south-eastern Tunisia. *Appl Water Sci* 3(2):415–429
- Ahmadi R, Mercier E, Ouali J (2013) Growth-strata geometry in fault-propagation folds: a case study from the Gafsa basin, southern Tunisian Atlas. *Swiss J Geosci* 106, 91–107
- Ali MBH, Jedoui Y, Dali T, Salem HB, Memmi L, 1985. Carte géologique à l'échelle 1/500,000 de la Tunisie. *Serv. Géol. Tunisie*
- Ben Ayed N, Viguier C (1981) Interprétation structurale de la Tunisie atlasique. *CRAS Paris* 292:1445–1448
- Bedir M, Tlig S, Bobier C, Aissaoui N (1996) Sequence stratigraphy, basin dynamics, and petroleum geology of the Miocene from eastern Tunisia. *AAPG Bull* 80(1):63–80
- Ben Hassen M, Deffontaines B, Turki MM (2014) Recent tectonic activity of the Gafsa fault through morphometric analysis: Southern Atlas of Tunisia. *Quatern Int* 338:99–112
- Ben Salem H, Chaouachi A, 1985. Carte géologique de Gafsa, CPG, ONM
- Bouaziz S, Barrier E, Angelier J, Tricart P, Turki MM (1998) Tectonic evolution of the Southern Tethyan margin in Southern Tunisia. *Mémoires Du Muséum National D'histoire Naturelle* 1993(177):215–236
- Bouderbala A, Remini B (2014) Geophysical approach for assessment of seawater intrusion in the coastal aquifer of Wadi Nador (Tipaza, Algeria). *Acta Geophys* 62(6):1352–1372
- Bryant RG, Sellwood BW, Millington AC, Drake NA (1994) Marine-like potash evaporite formation on a continental playa: case study from Chott el Djerid, southern Tunisia. *Sed Geol* 90(3–4):269–291
- Burrollet PF (1956) Contribution à l'étude stratigraphique de la Tunisie centrale. *Ann Mines Géol* 18:350
- Carreira PM, Marques JM, Nunes D (2014) Source of groundwater salinity in coastline aquifers based on environmental isotopes (Portugal): natural vs. human interference A review and reinterpretation. *Appl Geochem* 41:163–175
- Chabaane A, Redhaounia B, Gabtni H, Amiri A (2018) Contribution of geophysics to geometric characterization of freshwater–saltwater interface in the Maâmoura region (NE Tunisia). *Euro-Mediterranean J Environ Integr* 3(1):26
- Chongo M, Wibroe J, Staal-Thomsen K, Moses M, Nyambe IA, Larsen F, Bauer-Gottwein P (2011) The use of time domain electromagnetic method and continuous vertical electrical sounding to map groundwater salinity in the Barotse sub-basin, Zambia. *Physics and Chemistry of the Earth, Parts A/B/C* 36 (14–15), 798–805.
- Davis M (1986) Pharmacological and anatomical analysis of fear conditioning using the fear-potentiated startle paradigm. *Behav Neurosci* 100(6):814
- Delleur JW (Ed.) (2006) *The handbook of groundwater engineering*. CRC press
- Ebraheem AAM, Senosy MM, Dahab KA (1997) Geoelectrical and hydrogeochemical studies for delineating ground-water contamination due to salt-water intrusion in the northern part of the Nile Delta Egypt. *Ground Water* 35(2):216
- Ekine AS, Osobonye GT (1996) Surface geoelectric sounding for the determination of aquifer characteristics in parts of bonny local government area of river state. *J Phys* 85:93–97
- El Mejri H, Moussa AB, Salem SH, Zouari K (2018) Hydrochemical investigation and quality assessment of groundwater in the BouHafna-Haffouz unconfined aquifers, Central Tunisia. *Aquifers: Matrix and Fluids*, 91
- Fadili A, Najib S, Mehdi K, Riss J, Malaurent P, Makan A (2017) Geoelectrical and hydrochemical study for the assessment of seawater intrusion evolution in coastal aquifers of Oualidia, Morocco. *J Appl Geophys* 146:178–187
- Farhat, H., 1984. Ressources en eau souterraine de Gafsa et d'El Ayai-cha. Directorate-General for Water Resources Research.
- Farid I, Zouari K, Kallali A (2012) Origine de la salinité des eaux du bassin Chougafiya (Tunisie). *Revue Des Sciences De L'eau/journal of Water Science* 25(3):255–274
- Fedrigoni L, Krimissa M, Zouari K, Maliki A, Zuppi GM (2001) Origin of the salinisation and hydrogeochemical behaviour of a phreatic aquifer suffering severe natural and anthropic constraints: an example from the Djebeniana aquifer (Tunisia). *Comptes rendus de l'Académie des Sciences. Serie2.Fascicule a. Sciences de la terre et des planètes/Earth and planetary sciences* 332(11), 665–671

- Gharbi M, Espurt N, Masrouhi A, Bellier O, Amari EA (2015) Style of Atlasic tectonic deformation and geodynamic evolution of the southern Tethyan margin, Tunisia: Marine and Petroleum Geology 66,801–816
- Gouasmia M, Khorchani H, Mhamdi A, Dhahri F, Soussi M (2018) Hydrogeological characterization of a carbonate aquifer using geophysical and geochemical approach: case of the Krachoua Formation in Tataouine area Southern Tunisia. Arab J Geosci 11(24):786
- Gouasmia M (2008) Caractérisation de la géométrie des aquifères alluvionnaire, Néogène sableux et Crétacé carbonaté du bassin de Gafsa par les méthodes géophysiques. Thèse de Doctorat, Univ. Sfax, fac. Des Sc. Sfax, 221 p, 1 annexe
- Griffiths DH, Barker RD (1993) Two-dimensional resistivity imaging and modelling in areas of complex geology. J Appl Geophys 29(3–4):211–226
- Haji TA, Moumni Y, Msaddek MH (2020) Fault-style and seismic interpretation: implications for the structural issues of the Southeastern Atlas in Tunisia. J Afr Earth Sc 172(103962):11p
- Hamed Y, Ahmadi R, Demdoum A, Bouri S, Gargouri I, Dhia H, BChoura A (2014) Use of geochemical, isotopic, and age tracer data to develop models of groundwater flow: a case study of Gafsa mining basin-Southern Tunisia. J Afr Earth Sci 100, 418–436
- Houcine J, Friha HA, Kamel A, Kamel Z, Aggoune A (2014) Study of Rejim Maatoug groundwater in Southern Tunisia using isotope methods. J Hydro-Environ Res 8(3):316–327
- Karaouli F, Zammouri M, Tarhouni J, Hamed Y (2008) Étude hydrogéologique et impact de l'intensification de l'exploitation sur la qualité des eaux souterraines du bassin de Moularès-Redeyef (Sud-Ouest tunisien). Science Et Changements Planétaires/sécheresse 19(1):61–65
- Kraiem Z, Zouari K, Bencheikh N, Agoun A, Abidi B (2015) Processus de minéralisation de la nappe du Plio-Quaternaire dans la plaine de Segui-Zograta (Sud-Ouest tunisien). Hydrol Sci J 60(3):534–548
- Kraiem Z, Chkir N, Zouari K, Parisot JC, Agoun A, Hermitte D (2012) Tomographic, hydrochemical and isotopic investigations of the salinization processes in the oasis shallow aquifers, Nefzaoua region, southwestern Tunisia. J Earth Syst Sci 121(5):1185–1200
- Krimissa S, Michelot JL, Bouchaou L, Mudry J, Hsissou Y (2004) Sur l'origine par altération du substratum schisteux de la minéralisation chlorurée des eaux d'une nappe côtière sous climat semi-aride (Chtouka-Massa, Maroc). CR Geosci 336(15):1363–1369
- Li P, Qian H, Wu J, Zhang Y, Zhang H (2013) Major ion chemistry of shallow groundwater in the Dongsheng Coalfield, Ordos Basin China. Mine Water Environ 32(3):195–206
- Lotfi D, Yann L, Gerhard S, Mohamed H, Rajouene M (2018) Identifying the origin of groundwater salinisation in the Sidi El Hani basin (central-eastern Tunisia). J Afr Earth Sc 147:443–449
- Mamou, A., 1990. Caractéristiques, évaluation et gestion des ressources en eau du Sud-Tunisien. Doctoral dissertation, Paris 11.
- Mallick J, Singh CK, AlMesfer MK, Kumar A, Khan RA, Islam S, Rahman A (2018) Hydro geochemical assessment of groundwater quality in Aseer Region Saudi Arabia. Water 10(12):1847
- Masclé G, Arnaud H, Dardeau G, Debelmas J, Dubois P (1986) Halocinèse précoce sur la marge téthysienne alpine : vers une réinterprétation des zones de gypse des Alpes. Comptes rendus de l'Académie des sciences. Série 2, Mécanique, Physique, Chimie, Sciences de l'univers, Sciences de la Terre 302(15), 963–968
- Masoud AA (2014) Groundwater quality assessment of the shallow aquifers west of the Nile Delta (Egypt) using multivariate statistical and geostatistical techniques. J Afr Earth Sci 95:123–137
- Masrouhi A, Gharbi M, Bellier O, Ben Youssef M (2019) The Southern Atlas Front in Tunisia and its foreland basin: structural style and regional-scale deformation. Tectonophysics 764:1–24
- Marescot L (2004) Modélisation directe et inverse en prospection électrique sur les structures 3D complexes par la méthode des éléments finis (Doctoral dissertation, Universités de Nantes et de Lausanne)
- Marescot L, Monnet R, Chapellier D (2008) Resistivity and induced polarization surveys for slope instability studies in the Swiss Alps. Eng Geol 98(1–2):18–28
- Mhamdi A, Moussaoui I, Tarki M, Dassi L (2022) Assessment of groundwater mineralization processes in the Garâat Douza-Tebeddit shallow aquifer, Southwestern Tunisia: an integrated geoelectrical and hydrochemical approach. Carbonates Evaporites 37(2):1–16
- Mhamdi A, Dhahri F, Gouasmia M, Moumni L, Mohamed S (2015) Groundwater salinization survey of the Upper Cretaceous-Miocene Complex terminal aquifer in the Sabaa Biar area of southwestern Tunisia. J Afr Earth Sc 112:83–92
- Mhamdi A, Dhahri F, Gouasmia M, Inoubli N, Soussi M, Dhia HB (2013) Groundwater investigation in the southern part of Gabes using resistivity sounding, southern Tunisia. Arab J Geosci 6(2):601–614
- Mhamdi A, Gouasmia M, Gasmî M, Bouri S, Dhia HB (2006) Évaluation de la qualité de l'eau par application de la méthode géoélectrique: exemple de la plaine d'El Mida-Gabes nord (Sud tunisien). CR Geosci 338(16):1228–1239
- Mokadem N, Hamed Y, Hfaïd M, Dhia HB (2015) Hydrogeochemical and isotope evidence of groundwater evolution in El Guettar Oasis area Southwest Tunisia. Carbon Evaporites 30(4):417–437
- Mosaad S, Kehew AE (2019) Integration of geochemical data to assess the groundwater quality in a carbonate aquifer in the southeast of Beni-Suef city Egypt. J Afr Earth Sci 158:103558
- Moussaoui E, Mhamdi A, Gouasmia M, Dhahri F, Soussi M (2018) Contribution of hydrochemical and geoelectrical (ERT and VES) approaches to investigate salinization process of phreatic aquifer and climate change adaptation strategy in arid area: example of Garaat Douza and its proximities (Mediterranean Basin). In Conference of the Arabian Journal of Geosciences 189–193. Springer
- Cham Nejad HT, Mumipour M, Kaboli R, Najib OA (2011) Vertical electrical sounding (VES) resistivity survey technique to explore groundwater in an arid region, southeast Iran. J Appl Sci 11(23):3765–3774
- Najib S, Fadili A, Mehdi K, Riss J, Makan A (2017) Contribution of hydrochemical and geoelectrical approaches to investigate salinization process and seawater intrusion in the coastal aquifers of Chaouia, Morocco. J Contam Hydrol 198:24–36
- Oyedele KF (2009) Total dissolved solids (TDS) mapping in groundwater using geophysical method. N. Y. Sci.J. 2 (3). ISSN 1554e0200
- Ouhamdouch S, Bahir M, Ouazar D, Carreira PM, Zouari K (2019) Evaluation of climate change impact on ground water from semi-arid environment (Essaouira Basin, Morocco) using integrated approaches. Environ Earth Sci 78(15):449
- Panteleit B, Kessels W, Kantor W, Schulz HD (2001) Geochemical characteristics of salinization-zones in the coastal aquifer test field (CAT-Field) in North-Germany. In: Proceeding of fifth International Conference on Saltwater Intrusion and Coastal Aquifers-Monitoring, Modeling, and Management, Essaouira, Morocco (pp. 23–25)
- Piper AM (1994) A geographic procedure in the geochemical interpretation of water analysis. Trans Geophys Union 25:914–928
- Pulido-Leboeuf P, Pulido-Bosch A, Calvache ML, Vallejos A, Andreu JM (2003) Strontium, SO₄²⁻/Cl⁻ and Mg²⁺/Ca²⁺ ratios as tracers for the evolution of seawater into coastal aquifers: the example of Castell de Ferro aquifer (SE Spain). CR Geosci 335(14):1039–1048

- Ricolvi M (1976) Etude hydrogéologique de la nappe du crétacé inférieur de Gafsa. Document ARE, 26
- Schoeller H (1965) Hydrodynamique dans le karst [Hydrodynamics of karst]. In : Actes du Colloques de Dubrovnik. IAHS/ UNESCO, Wallingford, pp. 3–20
- Riley P, Gordon C, Simo JA, Tikoff B, Soussi M (2011) Structure of the Alima and associated anticlines in the foreland basin of the southern Atlas Mountains Tunisia. *Lithosphere* 3(1):76–91
- Shtivelman V, Goldman M (2000) Integration of shallow reflection seismics and time domain electromagnetics for detailed study of the coastal aquifer in the Nitzanim area of Israel. *J Appl Geophys* 44(2–3):197–215
- Sikandar P, Bakhsh A, Ali T, Arshad M (2010) Vertical electrical sounding (VES) resistivity survey technique to explore low salinity groundwater for tube well installation in Chaj Doab. *J Agric Res* 48(4):03681157
- Semar A, Hartani T, Bachir H (2019) Soil and water salinity evaluation in new agriculture land under arid climate, the case of the Hassi Miloud area, Algeria: Euro-Mediterranean *J Environ Integr* 4(1), 40, 14p
- Song SH, Lee JY, Park N (2007) Use of vertical electrical soundings to delineate seawater intrusion in a coastal area of Byunsan Korea. *Environ Geol* 52(6):1207–1219
- Soumaya A, Kadri A, Ayed NB, Kim YS, Dooley TP, Rajabi M, Braham A (2020) Deformation styles related to intraplate strike-slip fault systems of the Saharan-Tunisian Southern Atlas (North Africa): new kinematic models. *J Struct Geol* 140:104175
- Soumaya A, Ben Ayed N, Rajabi M, Meghraoui M, Delvaux D, Kadri A, Braham A (2018) Active faulting geometry and stress pattern near complex strike-slip systems along the Maghreb region: constraints on active convergence in the Western Mediterranean. *Tectonics* 37(9):3148–3173
- Soumaya A, Ben Ayed N, Delvaux D, Ghanmi M (2015) Spatial variation of present-day stress field and tectonic regime in Tunisia and surroundings from formal inversion of focal mechanisms: geodynamic implications for central Mediterranean. *Tectonics* 34(6):1154–1180
- Sassi M (1974) La sédimentation phosphatée au Paléocène dans le Sud et le Centre-Ouest de la Tunisie. Thèse Sci. Orsay 294 p
- Swezey CS (2003) The role of climate in the creation and destruction of continental stratigraphic records: an example from the northern margin of the Sahara Desert, in: *Climate Controls on Stratigraphy* (C.B. Cecil and N.T. Edgar, eds.): SEPM (Society for Sedimentary Geology) Special Publication 77, 207–225
- Swezey CS (1996) Structural controls on Quaternary depocentres within the Chotts Trough region of southern Tunisia. *J Afr Earth Sc* 22(3):335–347
- Tarki M, Dassi L, Jedoui Y (2012) Groundwater composition and recharge origin in the shallow aquifer of the Djerid oases, southern Tunisia: implications of return flow. *Hydrol Sci J* 57(4):790–804
- Tarki M, Dassi L, Hamed Y, Jedoui Y (2011) Geochemical and isotopic composition of groundwater in the Complex Terminal aquifer in southwestern Tunisia, with emphasis on the mixing by vertical leakage. *Environ Earth Sci* 64(1), 85–95
- Tizro AT, Voudouris KS (2008) Groundwater quality in the semi-arid region of the Chahardouly basin West Iran. *Hydrol Process* 22(16):3066–3078
- Trabelsi F, Ben Mammou A, Tarhouni J, Ranieri G (2011) Geophysical and hydrochemical monitoring of saltwater intrusion: Nabeul–Hammamet coastal aquifer case study (Northeast, Tunisia). In: Sixth international conference of applied geophysics for environment and territorial system engineering, Iglesias-Sardinia, Italy (pp. 71–76)
- Trabelsi R, Zaïri M, Smida H, Dhia HB (2005) Salinisation des nappes côtières : cas de la nappe nord duSahel de Sfax Tunisie. *Comptes Rendus Geoscience* 337(5):515–524
- Zammouri M, Siegfried T, El-Fahem T, Kriâa S, Kinzelbach W (2007) Salinization of groundwater in the Nefzawa oases region, Tunisia: results of a regional-scale hydrogeologic approach. *Hydrogeol J* 15(7):1357–1375
- Zargouni F (1984) Style et chronologie des déformations des structures de l'Atlas tunisien méridional. Évolution récente de l'accident Sud-atlasique. *Comptes rendus des séances de l'Académie des sciences. Série 2, Mécanique, Physique, Chimie, Sciences de l'univers, Sciences de la terre* 299(2), 71–76
- Zargouni F, Rabia MC, Abbes C (1985) Rôle des couloirs de cisaillement de Gafsa et de Negrine-Tozeur dans la structuration du faisceau des plis des Chott, éléments de l'accident sud-atlasique. *Comptes rendus de l'Académie des sciences. Série 2, Mécanique, Physique, Chimie, Sciences de l'univers, Sciences de la Terre* 301(11), 831–834
- Zouari K, Kamel S, Chkir N (2006) Long-term dynamic isotope and hydrochemical changes in the deep aquifer of Complex Terminal (Southern Tunisia). *IAEA-TECDOC* 507:127–156
- Zouari H (1992) Les variations géométriques du plissement liées à la cinématique coulissante en relais des accidents préexistants : exemple de l'atlas méridional de Tunisie. *Comptes rendus de l'Académie des sciences. Série 2, Mécanique, Physique, Chimie, Sciences de l'univers, Sciences de la Terre* 314(7),699–702

Springer Nature or its licensor (e.g. a society or other partner) holds exclusive rights to this article under a publishing agreement with the author(s) or other rightsholder(s); author self-archiving of the accepted manuscript version of this article is solely governed by the terms of such publishing agreement and applicable law.